Zeitschrift: Helvetica Physica Acta

Band: 68 (1995)

Heft: 5

Vereinsnachrichten: Réunion d'automne de la Société Suisse de Physique = Herbsttagung der Schweizerischen Physikalischen Gesellschaft = Automn [i.e. autumn] meeting of the Swiss Physical Society

Autor: [s.n.]

Réunion d'Automne de la Société Suisse de Physique

Herbsttagung der Schweizerischen Physikalischen Gesellschaft

Automn Meeting of the Swiss Physical Society

September 7, 1995

Saint-Gall, Switzerland

Helv Phys Acta
Vol. 68 (1995)

0018-0238/95/050494-02$1.50+0.20/0

Magnetic Flux Measurement of Cobalt Nanowires by Electron Holography

C. Beeli[1], P. Stadelmann[1] and B. Doudin[2]

[1]Centre Interdépartemental de Microscopie Electronique
[2]Institut de Physique Experimentale
Ecole Polytechnique Fédérale de Lausanne, CH-1015 Lausanne, Switzerland

Off-axis electron holography has been used to measure and to visualize the magnetic flux of magnetic cobalt nanowires, synthesized by electrodeposition in porous membranes. As a result it is evident that the magnetic field of a single nanowire can be understood as a superposition of magnetic dipoles oriented along the nanowire axis. The magnetic flux of single cobalt nanowires was found to correspond to integer multiples of $\Phi=h/e$, i.e. the magnetic flux of nanowires is quantized. We checked that the phase change measured was actually only due to the magnetic field, by taking a second hologram after reversing the specimen upside down.

Off-axis electron holography allows us to measure quantitatively the magnetic flux leaking from a magnetic specimen [1], and has been applied successfully to ferromagnetic microprobes [2] and micrometer sized barium ferrite particles [3]. Electrodeposition in nanoporous membranes has been shown to be a useful technique to make submicrometric particles of controlled morphology [4]. We report here a study of cobalt nanowires, with a radius of 40 ± 5 nm and a length of 1 to 6 μm, obtained by electrodeposition in track-etched polycarbonate foils [5,6]. The electron holograms were reconstructed using HoloWorks [7].

The phase images reconstructed from the holograms presented here have a maximum spatial resolution of 160 nm. The phase images were n-times amplified by representing the phase modulo $2\pi/n$ instead of modulo 2π. This technique, called phase difference amplification [1], is also amplifying the noise. According to the Aharonov-Bohm effect the phase difference between the object and the reference wave measured by electron holography corresponds to $\Delta\phi = e/h\iint \underline{B}\ \underline{n}\ dS$, where the integral is taken over the surface enclosed between the two electron trajectories [1,2]. It follows from this formula that a phase change of 2π corresponds to a magnetic flux of $\Phi=h/e$.

We have shown that the magnetic flux of cobalt nanowires is quantized in units of $\Phi=h/e$ [8]. Furthermore, the magnetization of the nanowires is not uniform. It can be described by a collinear superposition of dipoles of different lengths each with a flux of Φ [8].

We check that apart from localized disturbances by fragments lying on the carbon foil, the phase change was exclusively due to the magnetic flux of the nanowires, by taking a second hologram of the same nanowire after reversing the specimen [9] upside down (Figs. 1a and b). The phase difference measured in the first hologram corresponds to $\Delta\phi = \Delta\phi_{electr} + \Delta\phi_{magn}$, i.e. the phase difference contributions of magnetic and electric fields (mean inner potential and possible charging effects of the specimen) are additive. After reversing the specimen, the phase difference due to the magnetic flux changes sign, since the direction of the magnetization has been reversed with respect to the direction of the electron beam: $\Delta\phi = \Delta\phi_{electr} - \Delta\phi_{magn}$. The product $\Psi_E = \Psi_a \Psi_b$ of the two complex wave functions reconstructed from the two holograms, respectively the ratio $\Psi_M = \Psi_a / \Psi_b$, is used to separate the contribution of the magnetic field from the electric contributions. The phase image calculated from Ψ_E corresponds to a phase change $\Delta\phi_E = \Delta\phi_a + \Delta\phi_b = 2\Delta\phi_{electr}$, i.e. it is a two times phase amplified image of the electric contribution (Fig. 2a). Only at the position of the nanowire a phase change can be recognized in this image, indicating a phase change of the electrons which travelled through the nanowire and the absence an electric field due to charging. By contrast, the phase image calculated from the ratio Ψ_M of the two wave functions corresponds to a phase change $\Delta\phi_M = \Delta\phi_a - \Delta\phi_b = 2\Delta\phi_{magn}$, i.e. it is a two times phase amplified image of the magnetic contribution (Fig. 2b). Figs. 2c and d is a comparison of two 8 times phase amplified images calculated from Fig. 2b, respectively directly from the hologram in Fig. 1b. Both images show a very similar distribution of magnetic flux lines, confirming that the phase image of a hologram shows actually the contribution due to the magnetic flux of the nanowire. Note that the

nanowire studied here has a magnetic flux of $\Phi=h/e$, since eight equiphase lines join at the two poles of the nanowire. The quantization of the magnetic flux has been verified with a precision of $\Phi/32$ which corresponds also to the absolute precision of the phase measurement [7].

One of the authors (C.B.) acknowledges helpful discussions with G. Matteucci on the separation of electric and magnetic field contributions by electron holography.

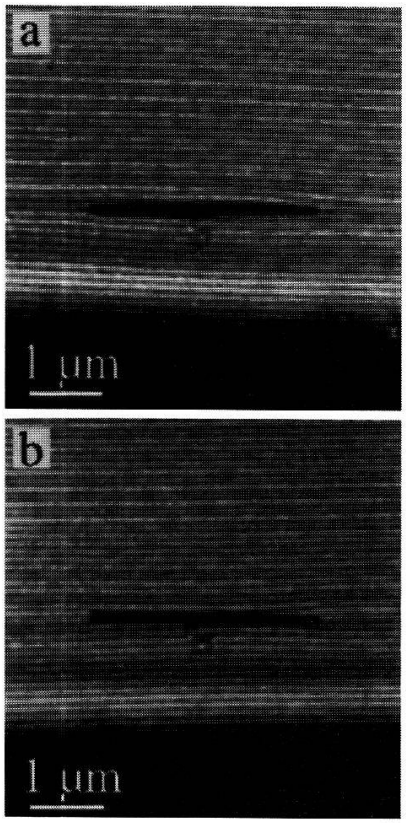

Fig. 1

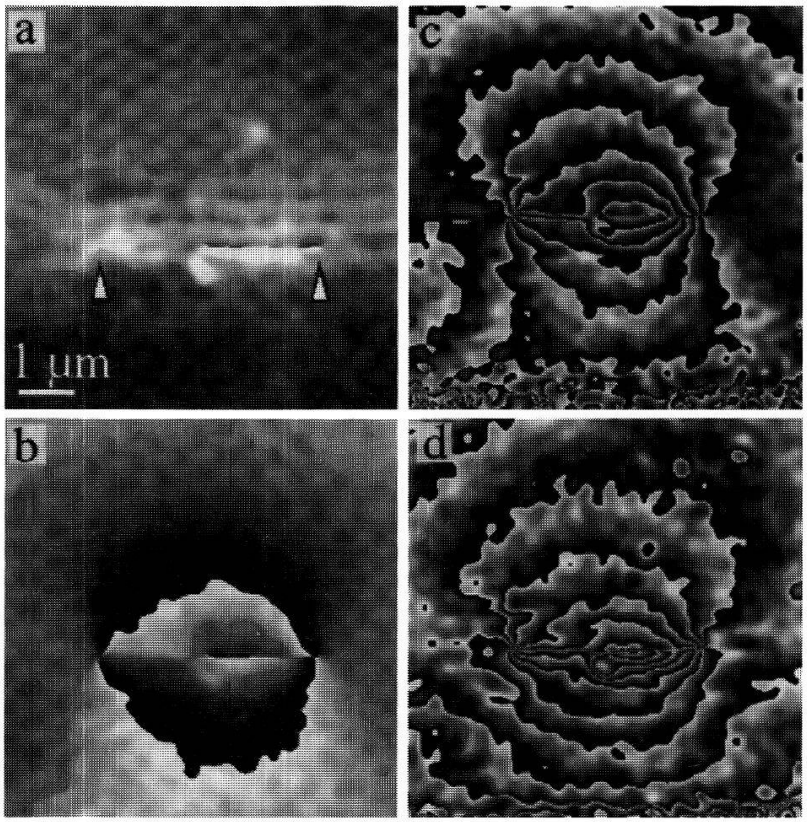

Fig. 2

Fig. 1 Two electron holograms of the same 3 μm long cobalt nanowire. 1b has been obtained after reversing the specimen upside down.

Fig. 2 a Phase image of the electric contribution (2 × amplified). Arrows indicate the ends of the wire.
b Phase image of the magnetic contribution (2 × amplified)
c Eight times phase amplified image obtained from 2b by additionally amplifying it four times
d Eight times phase amplified image reconstructed directly from the hologram 1b

[1] A. Tonomura, Electron Holography, Springer Series in Optical Sciences Vol. 70, (Springer, 1993)
[2] G. Matteucci, M. Muccini, and U. Hartmann, Phys. Rev. **B50**, 6823 (1994).
[3] T. Hirayama, Q. Ru, T. Tanji, and A. Tonomura, Appl. Phys. Lett. **63**, 418 (1993).
[4] B. Doudin and J.-Ph. Ansermet, NanoStructured Mater. **6**, 521 (1995)
[5] Poretics Corp., 111 Lindbergh Av., Livermore, CA 94550-9520
[6] C.R. Martin, Science **266**, 1961 (1994)
[7] E. Völkl and L. Allard, to appear in J. Microscopy (1995)
[8] C. Beeli, B. Doudin and P. Stadelmann, submitted to Phys. Rev. Lett. (1995)
[9] A. Tonomura, T. Matsuda, J. Endo, T. Arii, K. Mihama, Phys. Rev. **B34**, 3397 (1986)

Helv Phys Acta
Vol. 68 (1995)

0018-0238/95/050496-02$1.50+0.20/0

Magnetoresistivity in Y-La-Ca-Mn-O thin films

D. Noy, J.-P. Ramseyer, R. Sum, H.P. Lang and H.-J. Güntherodt
Institute of Physics, University of Basel, Klingelbergstr. 82, CH-4056 Basel, Switzerland

Thin films of $Y_{0.07}La_{0.60}Ca_{0.33}MnO_x$ have been prepared by pulsed laser deposition onto $LaAlO_3(012)$ substrates at different laser repetition rates. Whereas at a rate of 2.1 Hz a resistivity change of $(R_H\text{-}R_0)/R_H > 350\%$ (at T=100 K and H=1.2 T) is observed, at 6 Hz no magnetoresistive effect is found. Scanning tunneling microscopy reveals that film morphology is continuous in the first case, and is characterized by column-growth in the second case leading to inferior electrical properties.

The recent discovery of a giant magnetoresistive effect in perovskite-like $La_{0.67}Ca_{0.33}MnO_x$ thin films [1] initiated widespread research activity. This so-called giant magnetoresistance (GMR) effect is characterized by its large magnetoresistance (MR) ratio $\Delta R/R_H=(R_H\text{-}R_0)/R_H$, where R_0 is the resistance at a magnetic field H=0, and R_H is the resistance at a magnetic field H. The MR ratio is generally observed to be negative, and the effect is isotropic (i.e. independent of field orientation). Furthermore a strong temperature dependence of the MR ratio is found, with a MR ratio of more than 1500% at about 240 K (H=6T). Partial substitution of La by Y leads to an even larger MR ratio of more than 10'000% in thin films of the compound $Y_{0.07}La_{0.60}Ca_{0.33}MnO_x$ (YLCMO), but the temperature of the largest MR effect is shifted to 140 K (H=6T) [2].

A suitable method to grow thin films of high quality is pulsed laser deposition. We have used a KrF excimer laser (Lambda Physik LPX 301i, λ=248 nm, 1.5 J/cm^2). A polycrystalline YLCMO pellet prepared by a solid state reaction (12 h at 900°C and 4 h at 1400°C in flowing oxygen with intermediate grinding) of a mixture of La_2O_3, CaO, Mn_2O_3 and Y_2O_3 in appropriate amounts was used as target. Thin films of YLCMO have been grown on $LaAlO_3(012)$ polished single crystalline substrates at a deposition temperature of 700°C and an oxygen partial pressure of 25 Pa. A characterization of the samples by x-ray diffraction revealed that the thin films are epitaxial with YLCMO (001) parallel to $LaAlO_3(012)$. Imaging of the cross-section of the films using a scanning electron microscope yielded film thicknesses of ≈150 nm (see fig. 2). Resistivity of the thin films was determined by a standard 4-terminal resistivity measurement in the field (0-2 T) of an electromagnet (magnetic field perpendicular to the cur-

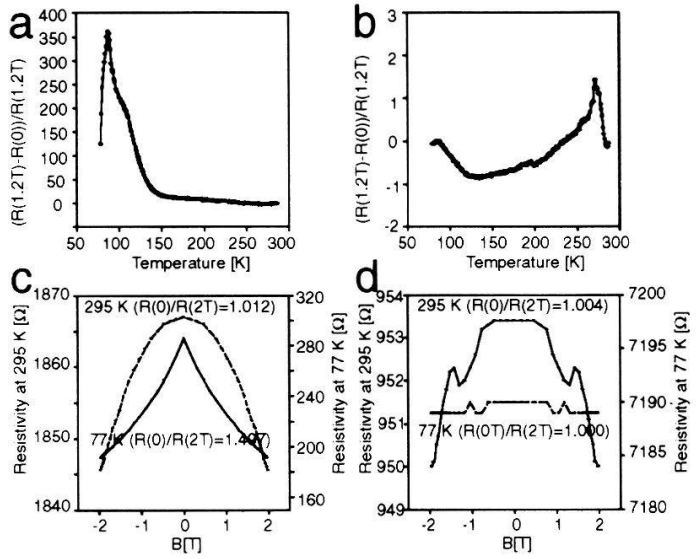

Fig. 1: Temperature-dependence of the MR ratio for YLCMO films prepared at a laser repetition rate of (a) 2.1 Hz, (b) 6 Hz. Magnetic field dependence of the resistivity at 77 K and 295 K for (c) the 2.1 Hz sample and (d) the 6 Hz sample.

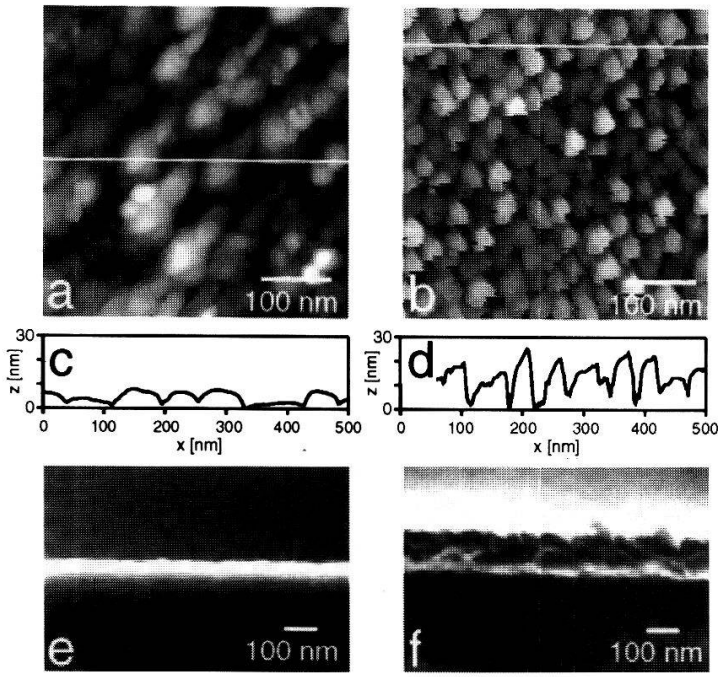

Fig. 2: STM topview images of the 2.1 Hz (a) and 6 Hz (b) samples. The white line refers to the sections shown in (c) and (d). Cross-section SEM images of the 2.1 Hz (e) and 6 Hz (f) films.

rent direction) in a temperature range between 77 K and ambient temperature. From the temperature-dependent resistivity in different magnetic fields, two types of curves were extracted. First, the MR ratio as a function of temperature, and second, the resistivity at 77 K and 295 K in dependence of the magnetic field. Figure 1 shows two sets of curves for thin films prepared at different laser repetition rates r. For the film prepared at r=2.1 Hz (fig. 1a) a clear magnetoresistive effect is observed (maximum of $\Delta R/R_H$ at $\approx$ 100 K). Surprisingly, no magnetoresistivity is found for the film prepared at r=6 Hz (fig. 1b). The 2.1 Hz sample shows the typical cusp-like behaviour of magnetic field dependence of the resistivity at 77 K as observed in [2] and a parabolic behaviour at 295 K (fig. 1c). The 6 Hz sample, however, exhibits only a very weak magnetic field dependence (fig. 1d). In order to clarify the striking difference in magnetoresistive behaviour between the two samples prepared at different laser repetition rates, morphological studies by scanning tunneling microscopy (STM) and scanning electron microscopy (SEM) have been performed. Figures 2a and 2b show the surface topography of the 2.1 Hz and 6 Hz YLCMO thin film samples. Whereas the 2.1 Hz sample exhibits a granular, but continuous surface, the 6 Hz sample consists of only weakly connected grains. The line section of the 2.1 Hz sample (fig. 2c) appears to be much smoother than the one of the 6 Hz sample (fig. 2d). The SEM cross-sections of the films reveal a smooth surface for the 2.1 Hz sample (fig. 2e) and columnar growth for the 6 Hz sample (fig. 2f). Due to the growth columns present in the 6 Hz sample, electrical current flow is hindered by the loose connection of the grains. Hence magnetoresistive behaviour is suppressed in the YLCMO thin film prepared at a laser repetition rate of 6 Hz.

The authors are grateful to D. Matthys (SEM Laboratory of the University of Basel) for supplying the SEM cross-section images.

REFERENCES

[1] S. Jin, T.H. Tiefel, M. McCormack, R.A. Fastnacht, R. Ramesh and L.H. Chen, Science **264**, 413 (1994).

[2] S. Jin, H.M. O'Bryan, T.H. Tiefel, M. McCormack and W.W. Rhodes, Appl. Phys. Lett. **66**, 382 (1995).

Helv Phys Acta
Vol. 68 (1995)

0018-0238/95/050498-02$1.50+0.20/0

Dielectric Investigation on CuO Single Crystals Phases Transitions

G.B. Parravicini and F. Marabelli
Dipartimento di Fisica "Volta", Università di Pavia, 27100 Pavia, Italy

Two magnetic transitions have been identified in CuO by several magnetic, thermodynamic and structural studies: at 230K to an incommensurate antiferromagnetic phase and at 212K to a commensurate one. Anyway the magnetic coordination has not been satisfactorily explained. In order to obtain further data on the nature of these phases, an investigation has been performed by means of dielectric measurements on single crystals, in the audiofrequency range and at temperatures ranging between 10 and 300K. Two peaks are detected corresponding to the transition temperatures and anomalies in the a.f.m. phase at 150 and 90-110 K are evidenced.

The cupric oxide CuO presents a double interest. It is commonly assumed that most of the properties of the copper-based HTSC depend on the interactions between copper and oxygen ions forming "chains" and plane structures. The square planar coordination is common to the cupric oxide structure. Moreover CuO is unique among the 3*d* transition-metal oxides both because of its monoclinic crystalline structure and because of the unusual magnetic properties which have not yet been fully explained. Numerous structural [1], thermodynamic[2] and magnetic [3] investigations have evidenced in CuO a paramagnetic to incommensurate antiferromagnetic transition at the temperature T=230 K and subsequently to commensurate ordering at 212 K. Unusually, the susceptibility continues to rise above the Néel temperature and reaches its maximum only at about 540 K. A clear anisotropy has been detected in magnetization measurements [4].

In order to gain further indications on the nature of the phase transitions, an experimental investigation was accomplished by means of dielectric measurements (as far as we know, the first obtained in CuO) in the temperature range 10-300 K, at frequencies 1000, 400 and 130 Hz. Due to the anisotropic character of the compound and in order to avoid the grain-grain interface effects, very considerable in polycrystalline samples, the experiments were performed on single crystals . Prism-shaped (0.8 x1x 8 mm^3) crystals were obtained, by the flux-growth method [5]. Further, a parallel structural investigation was performed by means of X-rays diffraction, in the temperature range 180-380 K, both to evaluate the "spurious" contribute to capacitance due to geometric thermal variations, and to investigate the possible singularities of the lattice parameters. For T=230K the lattice parameter along *a* and *b*-axes decreases with a larger slope, whereas it increases along the*c* -axis. Below T=212K, all parameters suddenly decrease with a larger rate.

The results of the dielectric measurements, performed with the electric field parallel to the *c*-axis, confirm the nature partially ionic of the Cu-O bond (calculated to be 43% [6]) and exhibit an evidence of the two phase transitions. A well defined peak both in capacitance and conductance appears, centred at T=231.3 K and about 4 K wide. A capacitance and

conductance peak was also detected, at T=211.3 K, about one order of magnitude less intense than the former and 0.5K wide. This temperature values have been found unchanged for the three explored frequencies. A quite similar response have been found in the other measured crystals obtaining small variations of the critical temperatures. In correspondence to the peaks, thermal emissions have been frequently revealed. In the a.f.m. phase, particularly at 200-180, 150 and 85-115 K, some explored samples evidenced further capacitance peaks analogous in amplitude to that at 230 K. Since X-rays diffraction escludes the presence of impurity phases, such anomalies can be ascribed to small deviation from oxygen stoichiometry.

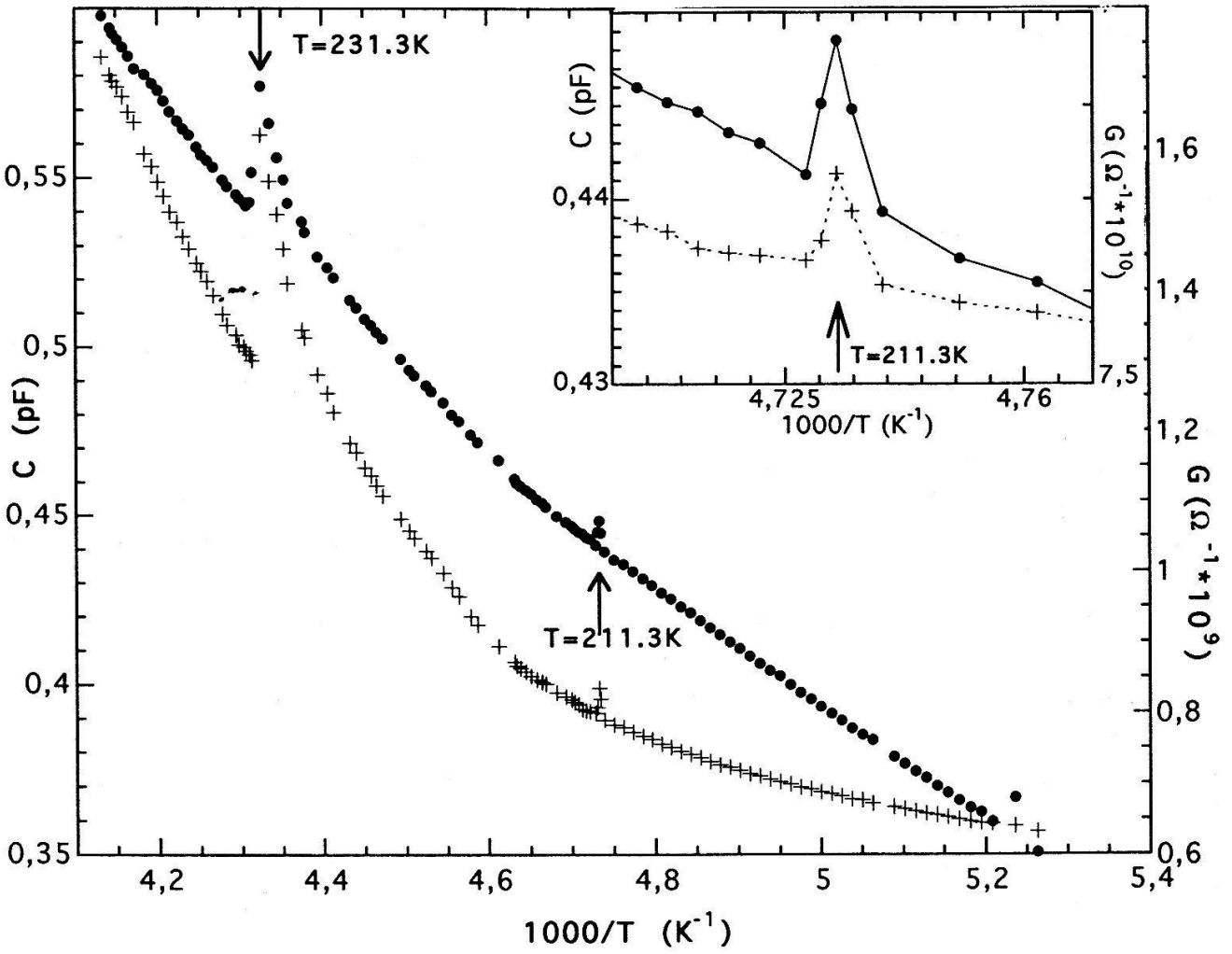

Fig. 1. Capacitance (•) and conductance (o) as a function of 1000/T for a CuO single crystal.

References

[1] J.B. Forsyth, P.J. Brown and B.M. Wanklyn, J. Phys. C, **21**, 2917 (1988).
[2] A. Junod, D. Eckert, G. Triscone et al, J. Phys: Condens. Matter **1**, 8021 (1989).
[3] S. Ota and E. Gmelin, Phys. Rev. B, **46,** 11632 (1992).
[4] F. Marabelli, G.B. Parravicini and P. Wachter , Solid State Comm. **86**, 131 (1993).
[5] B.M. Wanklyn and B.J. Garrard, J. Matter. Sci. Lett. **2**, 285 (1983).
[6] F. Lanza, R. Feduzi and J. Fuger, J. Mater; Res., **5**, 1739 (1990).

Helv Phys Acta
Vol. 68 (1995)

0018-0238/95/050500-02$1.50+0.20/0

Spatially–Resolved Tunneling Spectroscopy on $Bi_2Sr_2CaCu_2O_8$ Single Crystals

U. Hubler, P. Jess, S. Behler*, H.P. Lang, and H.-J. Güntherodt

Institute of Physics, University of Basel, Klingelbergstrasse 82, CH–4056 Basel, Switzerland
* present address: University of California, Lawrence Berkeley Laboratory, Materials Science Division, Berkeley CA 94720 USA.

The superconducting energy gap Δ of the high temperature superconductor $Bi_2Sr_2CaCu_2O_8$ is determined using a home–built high vacuum low temperature scanning tunneling microscope. From numerically derived dI/dV spectra acquired at different locations on the surface gap values of $\Delta = 31 \pm 5$ meV are obtained (Dynes fit). Other dI/dV curves show a V–shaped background suggesting a contamination layer present on the sample surface.

Besides electrical and magnetic properties of superconductors the determination of the superconducting energy gap is of major importance for the understanding of the pairing mechanism. One experimental method involves studies of current-voltage ($I(V)$) characteristics and their derivatives in macroscopic superconductor-insulator-normalconductor (SIN) junctions. The first derivative dI/dV of $I(V)$ characteristics is proportional to the superconductor's electronic density of states (DOS), thus revealing the energy gap when the device is at a temperature below the critical transition temperature T_c of the superconductor. To investigate local changes in $I(V)$ curves a scanning tunneling microscope (STM) is used representing a miniaturized tunneling contact of a sharp metallic tip, a vacuum tunneling barrier (insulator) and a superconductor surface.

Major issues in the investigation of high temperature superconductors (HTSC) based on layered cuprates involve nature and mechanism of pairing. A representative of HTSC that is built up of several copper oxide layers is $Bi_2Sr_2Ca_{n-1}Cu_nO_{2(n+2)}$ (n=1,2,3). Single crystals of the n=2 compound can easily be grown by a self-flux technique [1].

We have used a home-built STM which is operated in a high vacuum chamber (base pressure $< 10^{-6}$ mbar) situated in a bath cryostat suitable for temperatures down to 2.5 K. Prior to

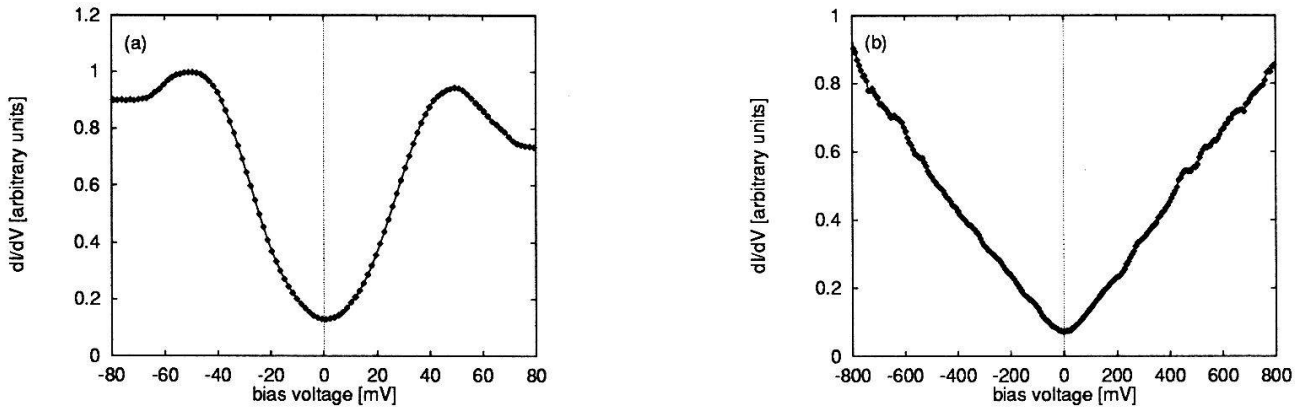

Figure 1: (a) dI/dV curve showing the energy gap of a BSCCO 2212 single crystal ($\Delta = 32.8 \pm 0.4$ meV). (b) dI/dV curve acquired at a different location. The V-shaped background implies the presence of a contamination layer. Further, no evidence of superconductivity is found here.

experiment the $Bi_2Sr_2CaCu_2O_8$ (BSCCO 2212) single crystal (1×1 mm^2) was cleaved along the (001) plane between two adjacent BiO planes and inserted into the STM under argon. Subsequently the STM was cooled down in high vacuum to 55 K within two hours by solidifying liquid nitrogen.

With a computer program especially developed for that purpose, $I(V)$ curves were acquired in different places on the surface.

Figure 1 shows two representative dI/dV curves (numerically derived from $I(V)$ data) out of a 16×16 grid acquired on a BSCCO 2212 surface. A clear gap structure is visible in fig. 1a. An evaluation using the Dynes equation $\frac{dI}{dV} \propto \left| \Re \frac{eV - i\Gamma}{\sqrt{(eV-i\Gamma)^2 - \Delta^2}} \right|$ yields $\Delta = 32.8 \pm 0.4$ meV (superconducting energy gap) and $\Gamma = 16.0 \pm 0.8$ meV (damping factor). This corresponds to a reduced energy gap of $\frac{2\Delta}{k_B T_c} \approx 9.3$ ($T_c = 82$ K). Being much larger than the BCS value in the weak coupling limit $\left(\frac{2\Delta}{k_B T_c} = 3.5\right)$ this value suggests strong electron-phonon coupling. Figure 1b depicts a dI/dV spectrum taken at a different location. Only a V-shaped background is observed here inferring the presence of a contamination layer [2]. The fact that different dI/dV spectra are found on different locations reflects the inhomogeneity of the sample surface due to surface degradation. For true vacuum tunneling an ohmic background as well as no dependence of the dI/dV characteristics on tunneling resistance or tip position would be expected.

To study the dependence of dI/dV spectra on tunneling resistance, a series of spectra was acquired at a position where a distinct gap structure could be observed. These dI/dV spectra are shown in figure 2a. No qualitative differences between spectra are found except for the differences in magnitude resulting from decreasing tunneling current with increasing tip-to-sample distance. This data normalized to $\frac{dI/dV(+80\text{mV})+dI/dV(-80\text{mV})}{2}$ is plotted in fig. 2b emphasizing identical qualitative behaviour. However, the background present in the dI/dV curves implies a contamination layer.

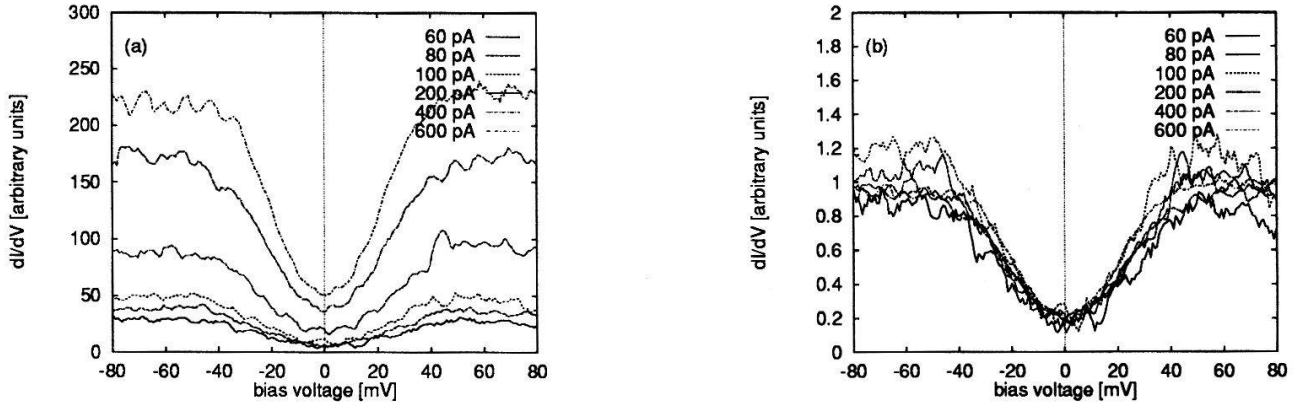

Figure 2: (a) dI/dV curves recorded at different tunneling currents. Due to the exponential decrease of the tunneling current with increasing tip-to-sample distance the spectra differ in magnitude, but not in shape. (b) Same data, but normalized to $\frac{dI/dV(+80\text{mV})+dI/dV(-80\text{mV})}{2}$.

In conclusion, it has been shown by scanning tunneling spectroscopy experiments that a reproducible superconducting gap feature $\Delta = 31 \pm 5$ meV is observed on BSCCO 2212 single crystals cleaved under argon. Since no qualitative dependence on the tunneling resistance is observed no direct tip-sample contact is assumed. However, the observation of V-shaped dI/dV curves as well as the background visible in all spectra suggests a contamination layer present on the sample surface.

REFERENCES

[1] H.P. Lang and H.-J. Güntherodt, Helv. Phys. Acta **66**, 65 (1993).
[2] Ch. Renner and Ø. Fischer, Phys. Rev. B **51**, 9208 (1995).

Helv Phys Acta
Vol. 68 (1995)

0018-0238/95/050502-02$1.50+0.20/0

Blue-green Laser by Frequency Doubling a Master Oscillator Power Amplifier Diode Laser in a $KNbO_3$ Crystal

Tomas Pliska, Daniel Fluck, and Peter Günter
Nonlinear Optics Laboratory, Institute of Quantum Electronics, Swiss Federal Institute of Technology, ETH Hönggerberg, CH-8093 Zürich, Switzerland

We report generation of 4.3mW coherent, diffraction-limited blue-green light at 491nm by single-pass frequency doubling of continuous-wave master oscillator power amplifier diode laser radiation in a 9.5mm long $KNbO_3$ crystal. A normalized conversion efficiency of up to $1.2\%W^{-1}cm^{-1}$ was reached. The root-mean-square fluctuations of the second harmonic output power was found to be as low as 0.1% and the long-term drift over 6 hours was ±1%.

Compact solid-state blue-green laser sources are of considerable technological interest for low-power applications in optical data storage, xerography and spectroscopy. Several schemes have been described for generating blue and green light by frequency doubling of near infrared diode lasers in nonlinear optical materials including resonant systems or waveguide devices. High power continuous-wave (cw) monolithic master oscillator power amplifier (M-MOPA) laser diodes [1], recently available from Spectra Diode Labs (SDL), allow to generate several milliwatts of blue-green radiation by frequency doubling in a simple single-pass scheme [2], [3], [4].

Potassium niobate ($KNbO_3$) proved to be very suitable for highly efficient second harmonic generation (SHG) into the blue-green spectral range with near infrared laser diodes thanks to its large nonlinear optical coefficients [5], [6], and its noncritical phase-matchability into the blue-green spectral range [7].

Results on SHG in $KNbO_3$ using the nonlinear optical coefficient d_{31} with a cw M-MOPA laser diode were reported previously. 3.7mW of blue-green power at 491nm were generated in a 8.2mm long crystal with a fundamental power of 1W and a normalized conversion efficiency of $0.5\%W^{-1}cm^{-1}$ [3]. At a lower power level a conversion efficiency of $0.7\%W^{-1}cm^{-1}$ was measured in a 7mm long crystal [4].

In this letter we report on second harmonic generation in a $KNbO_3$ crystal using the d_{31} coefficient performed with a 982nm M-MOPA diode. The M-MOPA laser diode (SDL-5762) was driven by an ILX LIGHTWAVE laser diode controller (LDC-3900). Its output power was 715mW when operated with an oscillator current of 195mA and an amplifier current of 2500mA. The emission wavelength was 981.6nm at an operating temperature of 22.7°C. The emission spectrum was analyzed with a scanning Fabry-Perot (BURLEIGH optical spectrum analyzer LD-800). The full-width-half-maximum (fwhm) bandwidth of the emission peak was less than the device resolution of 30GHz (0.1nm). The M^2-parameter of the beam was found to be close to 1 for both directions. In order to suppress any retro-reflections from optical components into the diode laser an optical isolator (ISOWAVE I-98-T5M, 49dB) was used. The transmission loss in the isolator was 0.6dB. The $KNbO_3$ crystal was mounted on a Peltier element, and the temperature was kept stable to ±0.05°C by a temperature controller.

The $KNbO_3$ crystal used for this work was grown in our laboratory by the top-seeded-solution-growth method. The b-faces were polished to $\lambda/8$ and anti-reflection coated at 980nm with a residual surface reflection loss of less than 1%. The surface reflection loss at 490nm was 22%. The length was 9.5mm.

The beam was focused into the crystal with an f=60mm lens to accomplish optimum focusing. Fig. 1 shows the second harmonic power as a function of the fundamental power. With a fundamental power of 612mW incident on the crystal a maximum second harmonic power of 4.3mW at 490.8nm was generated. This value includes the correction for the reflection loss at the crystal face at the second harmonic wavelength. The normalized conversion efficiency was $1.2\%W^{-1}cm^{-1}$. The crystal was kept at a temperature of 18.9°C.

The measurement of the M^2-parameter describing the far-field spreading of the second harmonic output beam yielded values of 1.0 and 1.1, respectively, for the two directions perpendicular to the beam propagation. We also investigated the temporal stability and noise of the second harmonic power output as shown in Fig. 2. Measured over a periode of more than six hours the power drift with respect to the mean second harmonic power was ±1%. The root-mean-square value of the amplitude fluctuations in the band between 10Hz and 100MHz was 0.1% of the average second harmonic power. The very good beam quality, low noise, and temporal stability make this type of blue-green source suitable for applications in optical recording.

We would like to thank H. Wüest for the crystal growth and J. Hajfler for the crystal polishing.

References

[1] D.F. Welch, R. Parke, D. Mehuys, A. Hardy, R. Lang, S. O'Brien, and D. Scifres, *Electron. Lett.* **28**, 2011-2013 (1992)

[2] L. Goldberg, L.E. Busse, and D. Mehuys, *Appl. Phys. Lett.* **63**, 2327-2329 (1993)

[3] R. Waarts, S. Sanders, R. Parke, D. Mehuys, R. Lang, S. O'Brien, K. Dzurko, D. Welch, and D. Scifres, *IEEE Photon. Technol. Lett.* **5**, 1122-1125 (1993)

[4] R. Waarts, R. Parke, D. Nam, D. Welch, D. Mehuys, R. Lang, S. O'Brien, K. Dzurko, and D. Scifres, *Proceedings Conference on Lasers and Electro-optics, Baltimore 1993*, 240-241 (paper CWC2) (1993)

[5] P. Günter, *Appl. Phys. Lett.* **34**, 650-652 (1979)

[6] J.-C. Baumert, J. Hoffnagle, and P. Günter, *SPIE* **492**, 374-385 (1984)

[7] I. Biaggio, P. Kerkoc, L.-S. Wu, P. Günter, and B. Zysset, *J. Opt. Soc. Am. B*, **9**, 507-517 (1992)

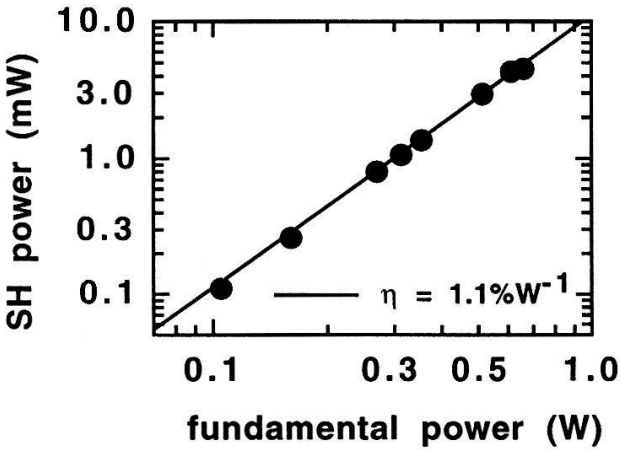

Fig. 1 Second harmonic power as a function of the incident fundamental power for frequency doubling MOPA laser diode radiation in a $KNbO_3$ crystal.

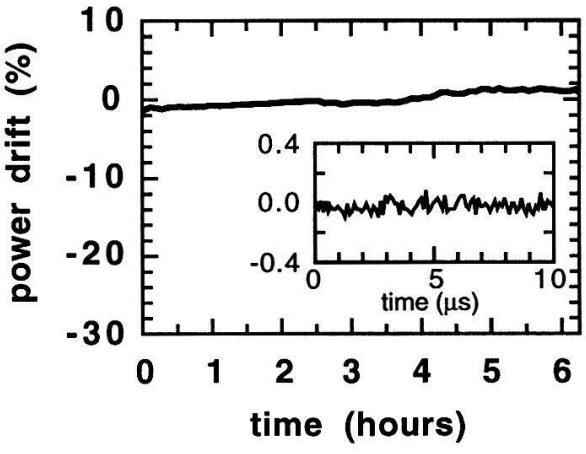

Fig. 2 Long-term power stability and short-term amplitude fluctuation (inset) of the second harmonic output power.

Helv Phys Acta
Vol. 68 (1995)

0018-0238/95/050504-02$1.50+0.20/0

Application of absorption measurements to the temperature determination of a cloud of cold Cesium atoms

Thomas Marty and Dieter Suter

Institute of Quantum Electronics, Eidgenössische Technische Hochschule Hönggerberg, CH-8093 Zürich, Switzerland

The temperature of a cloud of about 10^8 cold Cesium atoms in a magneto-optical trap has been determined with absorption measurements. On switching off the cooling laser, the atoms fall under gravity. The probe beam comes from a laser that is stabilized on the top of a dopplerfree saturated absorption line of a natural transition of Cesium. This laser serves to record absorption of the free falling atoms passing the probe beam positioned below the trapped cloud. By analysing the signal as a function of time and falling distance a cloud temperature of $1\,mK$ has been determined.

Testing samples of cold atoms by a probe laser beam opens a new field for spectroscopic activity. An important element for this type of experiment is the maximum absorption at a given falling distance and for a given sample. Absorption as a function of time of the free falling cloud passing a probe laser located below the trapped cloud has been recorded. The signal is known in the literature as Time-Of-Flight signal (TOF). It is usually observed by the probe induced fluorescence at falling distances of $1.1\,cm$ [1], $7\,cm$ [2] or $10\,cm$ [3]. Absorption measurements are suited for observation of the TOF signal at shorter falling distances up to $10\,mm$. The theory applied for the interpretation of the TOF signal obtained by absorption measurements is essentially the same as the one developed for the interpretation of the TOF signal obtained by the probe induced fluorescence [4].

Absorption spectra of a cold sample of Cesium atoms show three well resolved peaks corresponding to the natural transitions allowed by the selection rules $\Delta F = 0, \pm 1$. Highest absorption of 68% is measured in the trapped cloud, figure 1. The spectrum is recorded from the $F_g = 4$ groundstate with a probe intensity of $2\,mW/cm^2$.

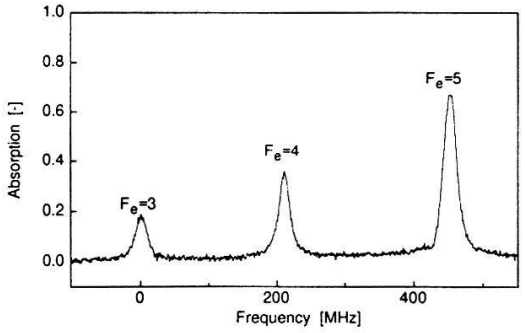

FIG. 1. Absorption spectrum of a trapped cloud of cold Cesium atoms showing only the natural transitions.

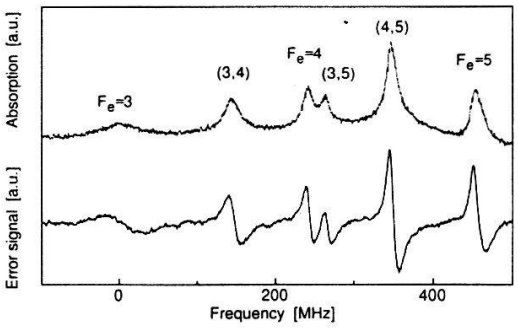

FIG. 2. Saturated absorption spectrum with error signal for stabilisation of the probe laser on the top of the $F_e = 5$ line.

To record the time-of-flight signal the probe laser is stabilized on the top of the dopplerfree saturated absorption line of the Cesium D_2 transition $F_g = 4 \rightarrow F_e = 5$. A recording of a typical saturated absorption spectrum with the simultaneously generated error signal used

for laser stabilisation is shown in figure 2. The necessary shift in optical frequency to generate the error signal is about $300\,KHz$, resulting in an absolute stability of the optical frequency of the same order.

A typical time-of-flight signal, measured with the absorption of the probe laser, is shown in figure 3. The power of the linear polarized probe beam is $5\,\mu W$ on an area of $0.8\,mm^2$. During recording the TOF signal, the cooling laser and the magnetic field were shut off. The repumping laser coupling to the $F_g = 3$ groundstate was on. This reduces hyperfine pumping of the free falling cloud by the probe laser. Temperature, falling distance and diameter of the trapped cloud were determined as fit parameters, taking into account the finite diameter of the probe laser. The TOF signal is mainly determined by temperature and falling distance. For the calculation of the fit, absorption is assumed to be proportional to particle density and temperature is introduced by the Maxwell-Boltzman distribution. On switching off the cooling laser the cloud starts falling under gravity according to Newton's law. This leads to a displacement of the whole distribution. It's height and width in time are mainly characterised by the temperature of the cloud and determine the TOF signal.

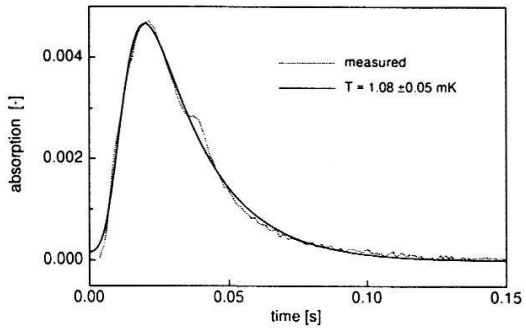

FIG. 3. Time-of-flight signal with curve fit to determine the temperature.

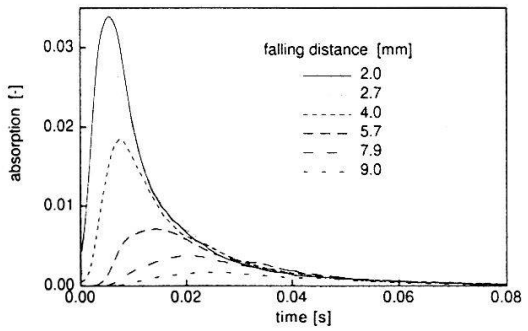

FIG. 4. Time-of-flight signals for different falling distances.

Figure 4 shows TOF signals for different falling distances. At short falling distances absorption is high. This is the range in which absorption measurements should be used for recording TOF signals. With increasing falling distance absorption decreases rapidly favouring the method of "probe induced fluorescence" [1, 2, 3, 4] for measuring TOF signals.

This work was financed by the "Schweizerischer Nationalfonds", by the Swiss Federal Institute of Technology and by Thomas Marty.

References

[1] P. Lett, R. Watts, C. Westbrook, W. Phillips, P.Gould, H. Metcalf: Phys. Rev. Lett. **61**, 169 (1988).

[2] C.Salomon, J.Dalibard, W.D.Phillips, A.Clairon, S. Guellati: Europhys. Lett. **12**, 683 (1990).

[3] M. Drewsen, Ph. Laurent, A. Nadir, G. Santarelli, A. Clairon, Y. Castin, D. Grison, C. Salomon: Appl. Phys. B **59**, 283 (1994).

[4] Weiss: J. Opt. Soc. Am. B **6**, 2082 (1989).

Helv Phys Acta
Vol. 68 (1995)

0018-0238/95/050506-02$1.50+0.20/0

Some aspects on the logarithmic law of the wall

Th. Kowalski and F. Ohle

Institut für Angewandte Mechanik und Strömungsphysik der Universität,
37073 Göttingen, Bunsenstr. 10, FRG

An experimental study of the logarithmic law of the wall in turbulent pipe flow is presented. The length of the pipe used for the investigation was 200 pipe-diameters. For the measured velocities in mean flow direction a distinctive wake region is found. Since the measurements have been carried out for Reynolds numbers of $33600 \leq Re \leq 210000$, the occurrence of such a wake region can be explained by a variety of different physical mechanism. Such mechanism will be discussed. The most interesting possibility for the existence of a wake region might be that the constants of the logarithmic law of the wall are not universal orthe turbulent flow is not fully developed, which is in contrast to other experimental studies.

The axisymmetric fully developed flow in a pipe provides one of the simplest and most reproducible laboratory flows for experimental wall-turbulence investigations. However, since Nikuradse [1] and Laufer [2] all turbulence hypotheses known so far have relied upon experimental studies, which show considerable inconsistencies. These inconsistencies can be interpreted by three separate physical criteria and characterize fully developed turbulent pipe flows. In general a fully turbulent flow exist when, first, the skin friction coefficient is related to the Reynolds number by an established law known to hold at high Reynolds numbers; second, the velocity distribution in the wall region follows the well known logarithmic law of the wall, i.e.

$$u^+ = \frac{1}{\kappa} \cdot \ln y^+ + C, \tag{1}$$

and third, the flow is continuously turbulent, i.e. no intermittency is presented. In Eq. (1) $u^+ = U/u_\tau$ defines the dimensionless velocity and $y^* = yu_\tau/\nu$ the dimensionless distance to the wall, u_τ is the friction velocity, ν is the kinematic viscosity, κ is the von Karman constant and C is an empirical constant. Coles [3] discussed the deviation of the velocity profile to the universal logarithmic law of the wall and introduced an improved version of Eq. (1), the law of the wake, which includes the dynamical properties of the so-called wake region. In this region a flow with a positive pressure gradient shows a characteristic deviation to the law of the wall at larger distances to the wall.

In this work an experimental study of the universal logarithmic law of the wall in turbulent pipe flow is presented. The measurements have been carried out in a circular pipe with a length of $L = 10.5m$ and a diameter of D=0.05m. More details of the experimental set up can be taken from Ref. [4]. Although a sufficient flow development length of $200D$ is used, where a fully turbulent state of the flow can be expected, deviations of the velocity profiles to the law of the wall are found. This phenomenon is illustrated in Fig. 1, where the development of the velocity component U in mean flow direction normalized with the friction velocity u_τ as a function of the normalized wall distance y^+ at $Re = U_{cl}D/\nu = 72000$ is presented (U_{cl} : centerline velocity). In the considered Reynolds number range all velocity profiles of the fully developed region show a significant deviation to the universal law of the wall. This phenomenon was also observed by other authors (see for example [5]). They assumed that such deviations are necessary to achieve a continuous transition of the law of the wall at the center of the pipe.

The constants $\kappa = 2.73$ and $C = 4.37$ derived from the experimental data also differ from the constants found in the literature, i.e. $\kappa = 2.5$ and $C = 5.5$. These deviations indicate that, if a universality of the constants κ and C is considered, the logarithmic law of the wall is valid only in the range of approximately $40 \leq y^+ \leq 200$, where the center of the pipe is at $y^+ = 1470$. The existence of a wake region and the deviation of the constants κ and C might be interpreted through the fact that the pipe flow is not fully developed. Since a linear pressure drop, which defines a characteristic property of a fully developed flow, is found above a flow development length of $100D$ this interpretation does not match with physical laws of turbulent flows [1,2]. If this result is considered in the discussion, then for such flows the constants κ and c might not be universal. Taking into account the development of both constants in dependence of the Reynolds number a good agreement to the fitted logarithmic law shown in Fig. 1 is obtained. This development can be explained by the continuous transition of the velocity profile in the center of the pipe. A larger value of κ similar to the one derived from the experimental data can also be calculated from the relation

$$\frac{U_{cl}}{u_\tau} = \frac{1}{\kappa} \ln \frac{u_\tau \cdot R}{\nu} + B \tag{2}$$

[6], where R defines the radius of the pipe and B is a constant, which can be neglected here. Using Eq. (2) $\kappa = 2.71$ and provides a good confirmation of the κ of Fig. 1.

In conclusion, when the pipe flow is fully developed, i.e. a linear pressure drop can be measured, then the question arises: Are the constants κ and C of the law of the wall universal or are they dependent on the experimental setup, or, what might be more interesting, are they dependent on the Reynolds number? Experiments along this line are in progress.

References

[1] J. Nikuradse, Forschungsheft 356, VDI-Verlag Berlin (1932)
[2] J. Laufer, N.A.C.A. tech. Rep. no. 1174 (1954)
[3] D. Coles, J. Fluid Mech. **1**, 191 (1956)
[4] Th. Kowalski, Mitteilung des MPI für Strömungsforschung, (1995)
[5] E. v. Driest, J. Aeronautical Sciences **23**, 1007 (1956)
[6] A.S. Monin and A.M. Yaglam, Statistical fluid mechanics: Mechanics of turbulence Vol. 1, MIT PRESS, Cambridge, (1979)

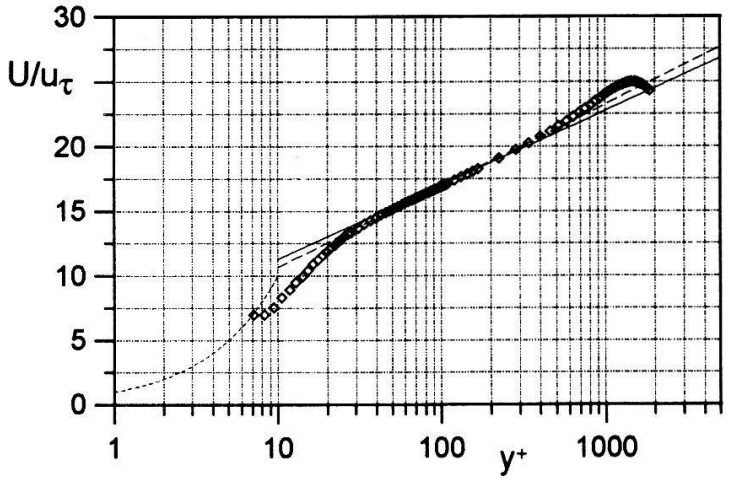

Fig. 1: Mean stream velocity U normalized with the friction velocity u_τ as a function of the normalized wall distance y^+ at $U_{cl} = 14\frac{m}{s}$. $\diamond$: experimental data, $\cdots$: viscose sublayer ($u^+ = y^+$), — : logarithmic law (Eq. 1), - -: fit to the present logarithmic law ($u^+ = 2.73 \ln y^+ + 4.37$)

Helv Phys Acta
Vol. 68 (1995)

0018-0238/95/050508-02$1.50+0.20/0

Estimation of the Landau coefficients for the dynamics of the periodic cylinder wake

F. Ohle and C.W. Heck

Institut für Angewandte Mechanik und Strömungsphysik der Universität,
37073 Göttingen, Bunsenstr. 10, FRG

It is well known that the periodic and transitional cylinder wake can be successfully modeled by a Ginzburg-Landau equation. In this work we discuss a method to estimate the corresponding Ginzburg-Landau coefficients. The model coefficients are extracted from measured time signals of the velocity fluctuations in the wake by the method of reconstruction of differential equations from experimental data. A systematic study of the regular cylinder wake for $53 \leq Re \leq 130$ is presented.

The wake behind a circular cylinder in the Reynolds number range of $50 \leq Re = U_\infty d/\nu \leq 160$, where U_∞ : mean stream velocity, d : cylinder diameter and ν : kinematic viscosity, is characterized by periodic vortex shedding. Today it is well established that such wake phenomena are well modeled by a Ginzburg Landau (GL) model with zero boundary conditions [1,2]. However, the determination of the model parameters are still not complete, because they depend on Re and from an experimental point of view, they are difficult to determine precisely. In this work a method is proposed to extract such parameters accurately.

The measurements have been carried out in the open-circuit type wind tunnel described in detail in Ref. [3]. It has been shown elsewhere [3-4] that the temporal dynamics of the periodic cylinder wakes can be described by a low-dimensional model (LDM) of the type

$$\ddot{u} = \sum_{\substack{i=0,\ldots,4 \\ j=0,\ldots,4-i}} a_{ij} u^i \dot{u}^j, \tag{1}$$

where u defines the velocity in mean flow direction, $\dot{u}$ and $\ddot{u}$ are its first and second time derivatives, and a_{ij} are the coefficients of a Taylor series expansion. The estimation of the GL parameters is based on the idea that for slowly varying amplitudes and frequencies, Eq. (1) can be approximated by the Stuart Landau (SL) equation

$$\dot{r} = \sigma_r r - l_r |r^2| r, \qquad \dot{\varphi} = \sigma_i - l_i r^2, \tag{2}$$

where the complex diffusive coupling term of the GL equation will not be considered [5]. In this equation r and $\omega := \dot{\varphi}$ are the amplitude and the angular frequency, and $\sigma = \sigma_r + i\sigma_i$ and $l = l_r + il_i$ are the complex linear and complex nonlinear coefficients. Such coefficients can be calculated from the reconstructed coefficients a_{ij} by a harmonic balance approximation, i.e.

$$\sigma_r = \frac{1}{2} a_{01}, \quad \sigma_i = -\frac{1}{8}(a_{21} + 3a_{03}), \quad l_r = \frac{1}{2}(1 - a_{10}), \quad l_i = -\frac{1}{8}(a_{12} + 3a_{30}). \tag{3}$$

The SL coefficients σ_r, l_r, $c_0 = \sigma_i/\sigma_r$, and $c_2 = l_r/l_i$ are globally dependent on the wake parameters $(Re, L/d)$, where L ist the length of the cylinder. The determination of c_0 is simple, since it affects the solution only be a frequency shift, and therefore can be deduced for example from parallel vortex shedding [2]. The coefficient c_2 can not be derived easily, because of the very high accuracy and great stability required. Even though the determination of c_0 and

c_2 depends on the wake dynamics, the advantage of the method presented here is that they can be calculated from the relations of Eq. (3). The small loss in accuracy results from the fact that the SL only considers systems with circular limit cycles in states space, whereas for the vortex street dynamics with increasing Re the attractor transforms from a circular to an asymmetric shape (Fig. 1.). In Fig. 2 the dependence of the GZ coefficients $|c_0|$ and $|c_2|$ from Re is shown. In general the values of c_0 calculated from the reconstructed coefficients (Eq. 3) differ up to four orders of magnitude to the ones estimated by other authors empirically [2]. Below $Re = 79$ the c_0 converges rapidly to a value of approximately one and with a further increase of the Reynolds number a very small continuous decrease of the c_0 is observed. The value of the coefficient c_2 known from the literature can only be reproduced for $Re < 60$, i.e. for $Re = 53$ we found $|c_2| = 2.2$. For $Re \geq 79$ the values of c_2 are found in the range of $0.01 \leq c_2 \leq 0.1$, which are two orders of magnitude smaller then the one considered in other works. Since good qualitative and quantitative predictions can be made by the reconstructed model (Eq. 1), the SL coefficients seem to be of high accuracy. This statement can be confirmed by calculating the frequency-amplitude coupling $\omega(r)$ near the asymptotic solution (r_0, ω_0). This coupling can be estimated by $\omega - \omega_0 = \Delta\omega = -2l_i(r - r_0)$. It can be seen in Fig. 3 that $\omega(r)$ shows a similar dependence on Re as the SL coefficient c_2 presented in Fig. 2.

References

[1] P. Albaréde and P.A. Monkewitz, Phys. Fluids A **4**, 744 (1992)
[2] P. Albaréde and M. Provansal, J. Fluid Mech. **291**, 191 (1995)
[3] F. Ohle and H. Eckelmann, Phys. Fluids A **4**, 1707 (1992)
[4] F. Ohle, Habilitationsschrift, in Vorbereitung (1995)
[5] Chr. Heck und F. Ohle, submitted to Phys. Rev. E (1995)

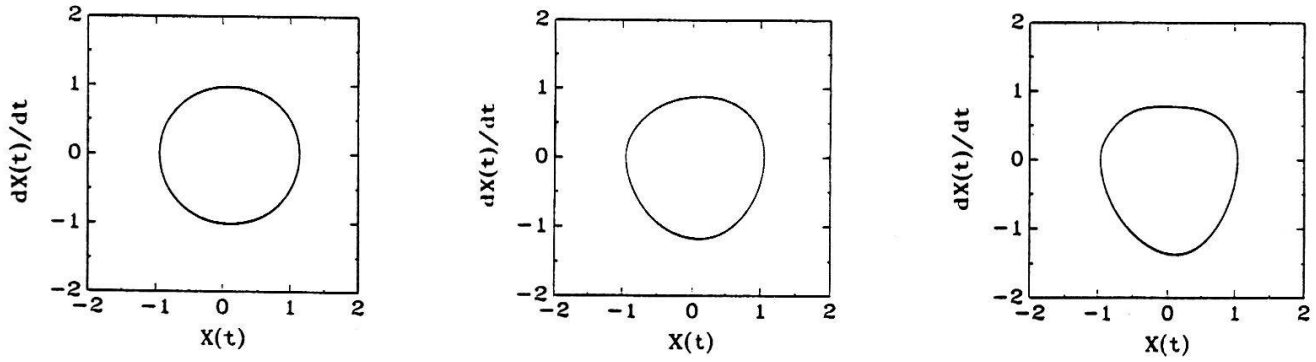

Fig. 1: State space reconstruction of three normalized dynamical states of a vortex street at $Re = 53$ (left), $Re = 99$ (middle) and $Re = 130$ (right).

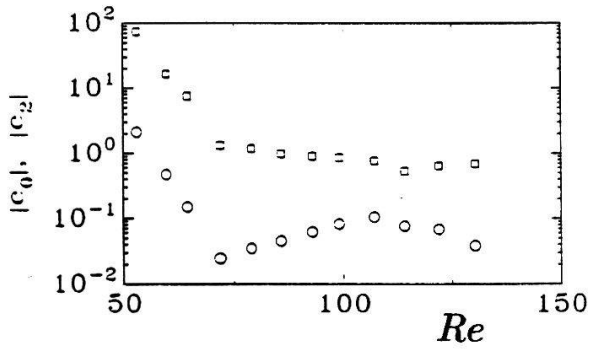

Fig. 2: Ginzburg-Landau coefficients $|c_0|$ (□) and $|c_2|$ (○) versus the Reynolds number.

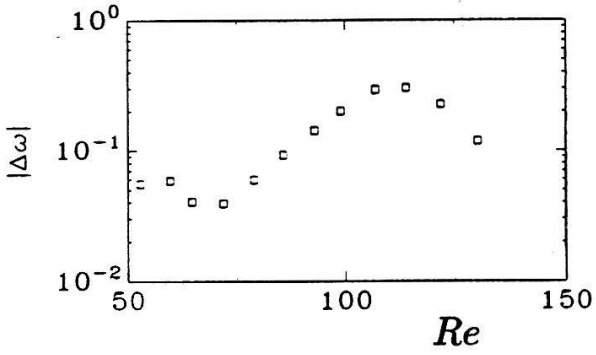

Fig. 3: Frequency-amplitude coupling $\Delta\omega$ versus the Reynolds number.

Helv Phys Acta
Vol. 68 (1995)

0018-0238/95/050510-02$1.50+0.20/0

Low-dimensional modeling of flutter instabilities

L. Völkering and F. Ohle

Institut für Angewandte Mechanik und Strömungsphysik der Universität,
37073 Göttingen, Bunsenstr. 10, FRG

Flutter phenomena arise from fluid forces induced by vibration of bluff or streamlined bodies in a fluid flow. In this work we discuss the possibility to extract low-dimensional models from the time evolution of the oscillatory motion of an airfoil. The numerical investigations presented here are focussed on a two-degree-of-freedom airfoil with a plunge and torsional mode. The advantage of this modeling is that physical parameters like the shape of the cross section, the stiffness or the viscous damping in plunge and torsion do not have to be measured or calculated explicitly.

The flutter phenomenon is a self-excited oscillation, caused by the interplay of aerodynamic elastic and inertia forces [1]. It describes a classical bifurcation phenomenon, where at a critical flow velocity the steady state of the system becomes unstable against an oscillatory state. Usually the term flutter is applied for at least two-degrees-of-freedom systems, where the structure is an airfoil in attached flow. Classical or binary flutter can occur even at small angle of attack and requires two elastic degrees of freedom the plunge (y) and torsional mode (Θ).

In the following, the dynamics of an experimental airfoil-configuration is simulated by a quasi-steady model for the aerodynamic forces restricted to small angles α [2,3]. The characteristic behavior of this airfoil, i.e. the dependence of the frequencies of plunge (f_y) and torsion (f_Θ) as a function of the velocity u and the corresponding angle α is shown in Fig. 1. It can be seen that at a certain velocity ($u_c \simeq 19\frac{m}{s}$) the frequency of the torsional mode locks into the frequency of the plunge mode. For $u < u_c$ both oscillatory motions are damped by the system. When $u > u_c$ the angle α increases and above a certain velocity limit cycle dynamics for the dynamics of plunge and torsion are obtained. The new ansatz to model such a dynamical system is based on the idea that these motions of plunge and torsion can be considered as a coupled dynamical system [3,4]. Its application starts with a state space reconstruction of the measured time signals of the plunge mode $y(t)$ and the torsional mode $\Theta(t)$. Fig. 2 shows the normalized state space reconstruction of a subcritical at $u = 10\frac{m}{s}$ and a supercritical dynamical state at $u = 30\frac{m}{s}$ of the considered airfoil (Fig. 1). From this representation a coupled system of two-dimensional ordinary differential equations of the type

$$\ddot{y} = \sum_{\substack{i,j,k,l,m=0,\ldots,3 \\ |i|+|j|+|k|+|l|+|m|\leq 3}} a_{ijklm} y^i \dot{y}^j \Theta^k \dot{\Theta}^l \ddot{\Theta}^m, \qquad \ddot{\Theta} = \sum_{\substack{i,j,k,l,m=0,\ldots,3 \\ |i|+|j|+|k|+|l|+|m|\leq 3}} b_{ijklm} y^i \dot{y}^j \Theta^k \dot{\Theta}^l \ddot{y}^m \qquad (1)$$

is reconstructed, where $\dot{y}$, $\ddot{y}$, $\dot{\Theta}$, and $\ddot{\Theta}$ are the first and second time derivatives of both modes, and a_{ijklm} and b_{ijklm} are the coefficients of the Taylor series expansions. For the modeling of the states of Fig. 2, a simplified ansatz is chosen, where instead of all 56 coefficients of Eq. (1) for each mode only 15 coefficients for the plunge and 4 for the torsion are fitted. This reduction is based on the assumption that the underlying equation of motion, from which the analysed data were simulated, are known. The reconstructed coefficients for the dynamical states of Fig. 2 are shown in Table 1. It can be seen that due to the coupling and the global dynamical change at u_c only a few coefficients show a stronger variation. Therefore, an accurate prediction of the development of the flutter instability is possible even when α is very small [3].

References

[1] R.D. Blevins, Flow-Induced Vibration, 2nd. ed., Van Nostrand Reinhold, NY (1990)
[2] F. Ohle, L. Völkering and G. Schewe, Helv. Phys. Acta **68**, 215 (1995)
[3] F. Ohle, Habilitationsschrift, in Vorbereitung (1995)
[4] Chr. Heck and F. Ohle, submitted to Phys. Rev. E (1995)

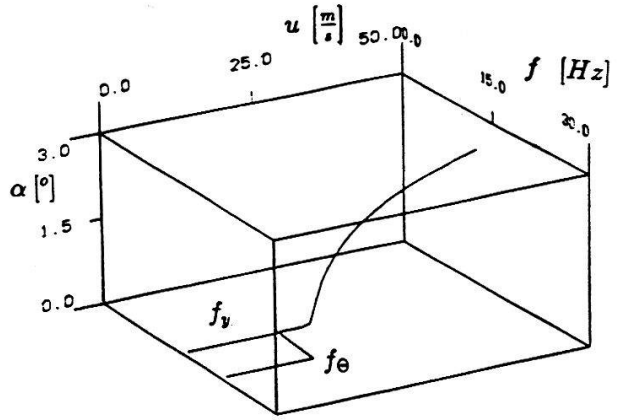

Fig. 1: Characteristic frequencies of plunge (f_y) and torsion (f_Θ) and the angle of attack (α) versus the velocity u for the considered airfoil-configuration (for more details see Ref. [2,3]).

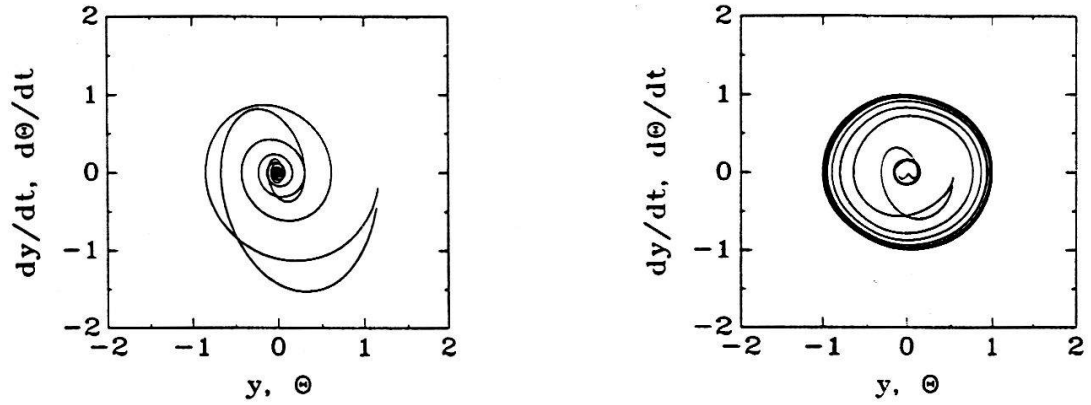

Fig. 2: State space reconstruction of the dynamics of the plunge and torsional mode for two different states. Left: subcritical state at $u = 10m/s$; right: supercritical state at $u = 30m/s$.

a, b	$u = 10m/s$		$u = 30m/s$	
ijklm	$y(t)$	$\Theta(t)$	$y(t)$	$\Theta(t)$
00001	-0.0858	-0.1455	-0.1353	-0.1452
00010	-0.0197	-0.4795	-0.0596	-0.5210
00100	-0.0399	-2.3837	0.0097	-2.1690
01000	-0.1747	0.0466	0.1366	0.1555
10000	-1.0976		-1.0143	
00030	0.0002		-0.0273	
00120	0.0037		-0.0485	
00210	0.0178		-0.0348	

continue:		
	$u = 10m/s$	$u = 30m/s$
ijklm	$y(t)$	$y(t)$
00300	0.0068	-0.0229
01020	0.0016	0.0310
01110	-0.0044	-0.0040
01200	-0.0226	-0.0772
02010	0.0125	0.0367
02100	-0.0043	-0.1765
03000	-0.0810	-0.1771

Table 1: Reconstructed coefficients of plunge ($y(t)$) and torsion ($\Theta(t)$) for the dynamical states shown in Fig. 2.